Nanoscale Structure and Structural Relaxation in Zr_{50}Cu_{45}Al_{5} Bulk Metallic Glass

Jinwoo Hwang, Z. H. Melgarejo, Y. E. Kalay, I. Kalay, M. J. Kramer, D. S. Stone, and P. M. Voyles

Phys. Rev. Lett. **108**, 195505 — Published 11 May 2012

DOI: 10.1103/PhysRevLett.108.195505

Nanoscale structure and structural relaxation in $Zr_{50}Cu_{45}Al_5$ bulk metallic glass

Jinwoo Hwang,[1,*] Z. H. Melgarejo,[1] Y. E. Kalay,[2,**] I. Kalay,[2,***] M. J. Kramer,[2] D. S. Stone,[1] and P. M. Voyles[1]

[1]Department of Materials Science and Engineering, University of Wisconsin, Madison, Madison Wisconsin 53706, USA

[2]Ames Laboratory (DOE), Ames, Iowa 50011, USA and Department of Materials Science and Engineering, Iowa State University, Ames, Iowa 50011, USA

*current address: Materials Department, University of California, Santa Barbara, Santa Barbara, California 93106-5050, USA

**current address: Department of Metallurgical and Materials Engineering, Middle East Technical University, Ankara, 06800 Turkey

*** current address: Department of Materials Science and Engineering, Cankaya University, Ankara, 06530, Turkey

Abstract

Hybrid reverse Monte Carlo simulations of the structure of $Zr_{50}Cu_{45}Al_5$ bulk metallic glass incorporating medium-range structure from fluctuation electron microscopy data and short-range structure from an embedded atom potential produce structures with significant fractions of icosahedral- and crystal-like atomic clusters. Similar clusters group together into nanometer-scale regions, and relaxation transforms crystal-like clusters into icosahedral clusters. A model refined against only the potential does not agree with the fluctuation microscopy data and contains few crystal-like clusters.

PACS: 61.43.Dq, 61.05.jm

A model of the structure of metallic glasses based on icosahedral-like, solute-centered nearest-neighbor clusters of atoms [1-5] has become widely accepted [6-11]. Icosahedral order has five-fold rotational symmetry that is incompatible with translational symmetry, so similar models have an extensive history [12-15]. Modern models include disordered icosahedra (thus "icosahedral-like") and focus on solute-centered clusters, which create chemical short-range order (SRO). Icosahedral-like models from reverse Monte Carlo (RMC) [1] and molecular dynamics (MD) simulations [5] are consistent with pair distribution function data. Beyond the nearest-neighbor clusters, these models contain little significant structure, although some specific packings of icosahedra have been proposed [3, 10, 11, 16]. Icosahedral-like clusters have been reported to play an important role in the glass transition [9] and plasticity [7].

In this Letter, we show that the icosahedral-like cluster model does not fully capture the structure of a real bulk metallic glass (BMG), although it may capture an idealized structure with maximum configurational entropy. By combining SRO from an empirical potential [5] with medium-range order (MRO) from fluctuation electron microscopy (FEM) data [17] in a hybrid RMC (HRMC) simulation [18], we show that, in additional to icosahedral-like clusters, $Zr_{50}Cu_{45}Al_5$ BMG contains a significant density of nearest-neighbor clusters with (potentially distorted) four- and six-fold rotational symmetry, which we call "crystal-like". Similar nearest-neighbor clusters, both crystal-like and icosahedral-like, group at medium-range, forming nanometer-scale superclusters, and the crystal-like superclusters favor fcc local bonding. Structural relaxation of a rapidly-quenched, high fictive temperature (T_f) glass below the glass transition temperature T_g reduces the fraction of crystal-like clusters and increases the fraction of icosahedral-like clusters, as does quenching the glass more slowly to a lower T_f.

FEM measures nanoscale structural fluctuations in glasses from the normalized variance, V, of many coherent nanodiffraction patterns [17], $V(k, R) = (\langle I^2(k, R, \mathbf{r})\rangle_{\mathbf{r}} / \langle I(k, R, \mathbf{r})\rangle^2_{\mathbf{r}}) - 1$. I is the diffracted intensity, $k = \sin(\theta)/\lambda$ is the scattering vector magnitude, R is the probe diameter, and $\langle\ \rangle_{\mathbf{r}}$ indicates averaging over position on the sample, $\mathbf{r}$. Quantitatively, V depends on the three- and four-atom distribution functions [17]. Qualitatively, heterogeneous nanoscale structure increases the spatial fluctuations in nanodiffraction, increasing V. The k position of peaks in $V(k)$ carries information about the internal structure of diffracting regions.

Previous interpretations of $V(k)$ data relied on creating an atomic model of a structural hypothesis, then simulating $V(k)$ [17, 19]. Hypotheses based on perfect icosahedral clusters do not match the FEM data for BMGs [20], so we have developed HRMC simulations that simultaneously minimize the χ^2 between the experimental and simulated $V(k)$ and the total energy E.

$$\chi^2 = E + \alpha \sum_i \frac{\left(\beta V_s(k_i) - V_e(k_i)\right)^2}{\sigma^2(k_i)}, \tag{1}$$

where V_s and V_e are the simulated and experimental variances, respectively, and σ is the uncertainty in V_e. We use an embedded atom model (EAM) potential for Zr-Cu-Al [5] to calculate E and the Dash *et al.* [21] method for V_s. Compared to previous RMC simulations incorporating FEM and $G(r)$ data [20, 22], minimizing E as well ensures realistic three dimensional physical and chemical SRO. Following [23], the proportionality factor α was adjusted over several simulations to make the contributions of E and V to χ^2 decrease at the same rate during minimization, achieving a minimum of both contributions simultaneously.

Equation (1) implies a quantitative comparison between V_s and V_e, which has been elusive: V_s is always larger than V_e [19, 24, 25]. Improved experiments reduce this discrepancy significantly. Our FEM experiments use nanodiffraction at 200 kV on a high-stability STEM, controlled, high probe coherence [26], zero-loss energy filtering [27], and constant sample thickness within ±0.5 nm [28]. The remaining difference in magnitude between V_e and V_s arises from the thickness, t, difference, and the Stobbs factor [17] including diffraction approximations [21], neither of which changes the shape of $V(k)$. For $t < 50$ nm, $V \propto 1/t$, [27, 29] and we assumed a typical correction factor of three [30]. The experimental thickness from the elastic electron transmittance [31] was 27 ± 2 nm, and the simulation thickness was 2.83 nm, making $\beta = 1/28.6$.

RMC is sensitive to initial conditions [32]. RMC incorporating FEM data reduces the solution space of possible models [20], but not to a structure with a unique position for every atom. The same dense-random packed (DRP) starting structure, created by MC minimization of a Lennard-Jones potential without even chemical SRO, was used for all the models. Starting from maximum disorder creates the minimally ordered models consistent with the FEM data, so our results are a lower bound on the possible structural order in the real materials. As a control, we created a model by MC minimization of E only, without the FEM data.

We studied ribbons of $Zr_{50}Cu_{45}Al_5$ BMG quenched by melt spinning at 30 m/s giving a quench rate of ~10^6 K/s [33] with T_g = 403 °C. As-quenched ribbons were annealed in a differential scanning calorimeter (DSC) at 300 °C ($0.85T_g$) for 10 minutes and 60 minutes, and remelted at 435 °C ($1.05T_g$) for 2 minutes, then cooled back into the glass at 0.33 K/s. All of the samples are completely amorphous to synchrotron (Fig. 2(b)) and electron diffraction (not shown). Fig. 1 shows DSC data with heat released below T_g in the as-quenched sample, typical

of relaxation of high T_f glasses [34]. Sub-T_g annealing reduced the heat release, indicating that the glass is structurally relaxed or aged. The low T_f sample is fully relaxed within the accuracy of the measurements.

Fig. 2(a) shows $V(k)$ data with R = 2 nm from these four specimens. STEM specimens were thinned by electropolishing, then 700 eV Ar ion milling to remove surface oxidation. Several hundred to a thousand nanodiffraction patterns were acquired for each sample. The annular average of each pattern was used to calculate V. The large peak in V falls entirely within the first peak in $S(k)$ (Fig. 2(b)), but there is a shift in the $V(k)$ peak maximum from 4.0 nm^{-1} in the as-quenched state to 3.7 nm^{-1} in the low T_f state, with the relaxed samples in between. Changes in $G(r)$ from a similar glass similarly relaxed are very small [35], implying limited changes in bond lengths and coordination numbers.

Fig. 2(a) also shows excellent agreement between $V_e(k)$ and $V_s(k)$ from HRMC models of 1,425 atoms in a $(2.83)^3$ nm^3 cubic box refined against all four $V_e(k)$ data sets. $V_s(k)$ from the EAM-only model shows no significant peaks, so it does not contain MRO consistent with experiment. $V_s(k)$ for a MD-quenched glass consisting of solute-centered clusters [35] has a similar lack of structure, and, scaled by the model thickness, similar magnitude to the EAM-only $V_s(k)$. Fig 2(b) shows the calculated structure factors, $S(k)$, from the EAM only model and the HRMC models, and the experimental $S(k)$ from synchrotron XRD on an as-quenched sample. Refinement against $V(k)$ did not significantly change the model's $S(k)$: all the HRMC models agree with the EAM-only model and with $S(k)$ of a $Zr_{47}Cu_{46}Al_7$ model quenched by MD with the same potential [5]. The partial $S(k)$'s of all five models (not shown) are also essentially the same. The difference in the peak positions between simulation and experiment corresponds to ~2.4% difference in interatomic spacings. The energy of the HRMC models is 17-20 meV/atom

higher than the EAM-only model, perhaps because the SRO encoded in $V(k)$ similarly disagrees slightly with the potential.

Fig. 3(a) shows the Voronoi polyhedra (VP) statistics [37] for the models. 96% of the VP were of the types ⟨0,0,12,0⟩, ⟨0,1,10,*x*⟩, ⟨0,2,8,*x*⟩, ⟨0,3,6,*x*⟩, ⟨0,4,4,*x*⟩, and ⟨0,5,2,*x*⟩, where x is typically between 0 and 4. No other single type constituted more than 1% of the VP. Following Cheng *et al.* [5] we group VP with many pentagonal faces, such as ⟨0,0,12,0⟩ and ⟨0,2,8,2⟩ as icosahedral-like. VP with many rectangular or hexagonal faces, such as ⟨0,4,4,*x*⟩ and ⟨0,5,2,*x*⟩, we call "crystal-like", because they can exhibit crystallographically allowed four- and six-fold rotational symmetry, and the ⟨0,3,6,*x*⟩ VP we call "mixed".

The EAM-only model has similar VP statistics to the MD model of Cheng *et al.* [5], so icosahedral-like VP seem to be a feature of the potential, independent of the model construction method. The fraction of crystal-like VP is small. The HRMC models showed more crystal-like VP and fewer icosahedral-like VP, which must be a consequence of the FEM data. Crystal-like VP have not been reported in significant fractions in previous BMG structural models.

Common neighbor analysis (CNA) using the Clarke and Jónnson notation [38], shown in Fig. 3(b), is similar. 555, the index of the bonds in a perfect icosahedron, shows the same pattern from model to model as the icosahedral-like VP. The HRMC models have significantly higher fractions of 422 and 421 CNA indices, the bonds in hcp and fcc crystals, than previous models [1], although there are no statistically significant changes with relaxation. 533 and 432 are distorted icosahedra [1], which also do not vary with relaxation. Indices not shown in Fig. 3(b) individually constitute <5% of the total.

Similar VP group together to form larger superclusters in the HRMC models. Fig. 4(a) shows part of the 300 °C, 60 minute HRMC model with the atoms colored by the fraction of pentagons in their VP, not by composition. In the center of the figure, the crystal-like VP form a supercluster which has approximate four- and six-fold rotational symmetry, viewed down the six-fold axis. Many of the icosahedral-like VP have formed superclusters with approximate two-fold symmetry, examples of which are circled in yellow and green. (Rotational symmetries are emphasized in the model's three-dimensional reciprocal space in the Supplementary Material [39]). In both cases, the atoms are arranged in clear, although disordered, planes. These pseudo-planes create the strong nanodiffraction which gives rise to the FEM $V(k)$ [20]; FEM is insensitive to other VP packings [36]. The size of the crystal-like superclusters in the models is 0.7 – 1.0 nm. However, that may not accurately represent the real material, due to the small size of our models, each of which contains only one crystal-like supercluster. Variable-resolution FEM experiments [17] and larger simulations are needed to determine the supercluster size. Unfortunately, larger models are prohibitively computationally expensive [20]. Fig 4(b) shows the EAM-only model, with no segregation of VP by type and no pseudo-planar structures. No similar structure with pseudo-planar order, distinct rotational symmetry, and nanometer size has been reported in MD quenched models, probably because the extremely high cooling rate in MD (10^{10} – 10^{13} K/s [5]) does not allow time for these larger structures to form.

The icosahedral-like supercluster has a plane spacing of 0.27 nm, as shown in Fig. 4(a), which corresponds to the peak in $V(k)$ at 3.7 nm^{-1}. The crystal-like supercluster has a plane spacing of 0.25 nm, corresponding to the peak at 4.0 nm^{-1}, but also shares the larger plane spacing. Thus, total VP fractions in the models are reliable, since they are constrained by the relative heights of the peaks in $V(k)$. In Fig 4(a), the vertical planes connect the icosahedral-like

and crystal-like superclusters, which may reflect the real structure, or may be a small-model artifact. The higher-k peaks may be other reflections of the same structures.

Although the VPs do not correspond to a simple crystal structure, CNA analysis indicates that the crystal-like supercluster is similar to an fcc crystal at the most local level. Fig. 4(c) shows that the crystal-like supercluster in the 300 °C for 60 minutes model has a much higher fraction of 421 indices than the remainder of the model. hcp has an equal number of 421 and 422 indices, so this indicates a locally fcc structure. Crystalline $ZrCu_2Al$ and ZrCuAl [40] have 421 CNA indices, but the crystal-like supercluster composition is no different from the total model, so it contains too little Al to correspond to these structures beyond the CNA length scale. The remainder of the model has a much higher percentage of 555 clusters. Comparison of the absolute number of indices in the whole model and the sub-models shows that the interface is dominated by distorted icosahedra, indices 544 and 433.

Fig. 4(d) shows the icosahedral cluster in the yellow circle in Fig. 4(a), which consists of a chain of primarily icosahedral-like VP and a few mixed VP, with various center atoms. Out of icosahedral superclusters that have been proposed [3, 11, 13], Fig. 4(c) is most like the structure proposed by Stephens and Goldman [41]. They sought to model diffraction from quasicrytals, so their structure contains planes of atoms that cause diffraction, which is also required for V.

Fig. 3(a) shows that the trajectory of the VP fractions during relaxation is from crystal-like, through mixed, to icosahedral-like as a function of the decreasing sub-T_g heat release. Since $S(k)$ is invariant, the change in VP types must be caused by the $V(k)$ peak shift in Fig. 2 from the 4 nm^{-1} peak associated with crystal-like VP to the 3.7 nm^{-1} peak associated with icosahedral-like VP. At 300 °C, the transformation proceeds slowly, with an intermediate stage of high mixed

and low crystal-like VP captured at 10 minutes. Above T_g, the transformation to icosahedral-like VP is complete in 2 minutes. The low T_f sample is also the most similar to the EAM model, suggesting that the EAM model may capture an ideal relaxed glass structure.

The mean energies per atom in the crystal-like and icosahedral-like superclusters within the HRMC models are statistically indistinguishable. Small differences in energy are difficult to detect due to the small number of atoms in the crystal-like superclusters, but the similarity in energy also reflects the poor internal ordering and small size of the crystal-like superclusters. Icosahedra are tight-packed, low-energy SRO structures for this potential [5], so crystals only become lower energy at larger size. Small size may also mean that even if these clusters have the right structure to be nuclei for crystallization, they are below the critical size, and thus tend to relax on annealing. The enthalpy released by relaxation may come from dissolving some crystal-like superclusters or from removing the internal interfaces between the crystal-like and icosahedral-like superclusters.

The existence of two distinct structural units is supported by BMG dynamics. Hu *et al.* [8] attributed anomalous enthalpy relaxation behavior in rapidly-quenched Zr-Cu-Al to at least two structural types with different β relaxation times, and Zhang *et al.* [42] have used two structural types to explain a fragile-to-strong crossover in the viscosity of BMG liquids. Since both icosahedral-like [7, 9] and crystal-like [43, 44] structural units have slow dynamics in simulations of different metallic glass liquids, perhaps both of the supercluster types we have identified contribute to slow dynamics in the liquid and thus to the glass transition. Additional simulations are required.

In summary, we propose a new model for the atomic structure of bulk metallic glasses based on hybrid reverse Monte Carlo modeling constrained at short range by an empirical interatomic potential and at medium range by fluctuation electron microscopy data. The model consists of superclusters of atoms in crystal-like local environments, as expressed by their Voronoi polyhedra, and chain superclusters of icosahedral-like Voronoi polyhedra. The existence of a significant fraction of crystal-like Voronoi polyhedra and clustering of like polyhedra at medium range are new features of this model. Structural relaxation of a rapidly-quenched glass with high fictive temperature decreases the fraction of crystal-like Voronoi polyhedra and increases the fraction of icosahedral-like Voronoi polyhedra, as does slower quenching to lower fictive temperature. These lower enthalpy structures are similar to a model refined against only the potential, suggesting that model represents an ideal, maximum entropy glass.

This work was supported by the National Science Foundation under contract CMMI-0824719 and by Teragrid award DMR-100061 (JH, ZM, DSS, and PMV). Alloys were synthesized at Ames Laboratory (MJK, EK and IK) supported by the U.S. Department of Energy, Office of Basic Energy Science, under Contract No. DE-AC02-07CH11358. Synchrotron data (MJK, EK and IK) were collected at the Advanced Photon Source supported under Contract No. DE-AC02-06CH11357. We thank Howard Sheng for assistance using the Zr-Cu-Al EAM potential.

References

[1] W. Luo, H. W. Sheng, F. Alamgir, J. Bai, J. He, and E. Ma, Phys. Rev. Lett. **92**, 145502 (2004).
[2] H. W. Sheng, W. K. Luo, F. M. Alamgir, J. M. Bai, and E. Ma., Nature **439**, 419 (2006).
[3] W. K. Luo, H. W. Sheng, and E. Ma, Appl. Phys. Lett. **89**, 131927 (2006).
[4] H. W. Sheng, Y. Q. Cheng, P. L. Lee, S. D. Shastri, and E. Ma, Acta Mater. **56**, 6264-6272 (2008).
[5] Y. Q. Cheng, E. Ma, and H. W. Sheng, Phys. Rev. Lett. **102**, 245501 (2009).
[6] T. Fujita, K. Konno, W. Zhang, V. Kumar, M. Matsuura, A. Inoue, T. Sakurai, M. Chen, Phys. Rev. Lett. **103**, 075502 (2009).
[7] N. Jakse, and A. Pasturel, Appl. Phys. Lett. **93**, 113104 (2008).
[8] L. Hu, Y. Yue, and C. Zhang, Appl. Phys. Lett. **98**, 081904 (2011).
[9] Y. Q. Cheng, E. Ma, and H. W. Sheng, Appl. Phys. Lett. **93**, 111913 (2008).
[10] D. B. Miracle, Nat. Mat. **3**, 697 (2004).
[11] D. Ma, A. D. Stoica, and X.-L. Wang, Nat. Mat. **8**, 30 (2009).
[12] J. D. Bernal, Proc. Roy. Soc. Lond. A **280**, 299 (1964).
[13] L. Cervinka, J. Non-Cryst. Sol. **156-158**, 94 (1993).
[14] C. L. Briant, and J. J. Burton, Phys. Stat. Sol. B **85**, 393 (1978).
[15] H. Jonsson, and H. C. Andersen, Phys. Rev. Lett. **60**, 2295 (1988).
[16] M. Li, et al., Phys. Rev. B **80**, 184201 (2009).
[17] M. M. J. Treacy, J. M. Gibson, L. Fan, D. J. Paterson, and I. McNulty, Rep. Prog. Phys. **68**, 2899 (2005).
[18] G. Opletal, T. C. Petersen, D. G. McCulloch, I. K. Snook, and I. Yarovsky, J. Phys. Cond. Mat. **17**, 2605 (2005).
[19] M. M. J. Treacy, J. M. Gibson, and P. J. Keblinski, J. Non-Cryst. Sol. **231**, 99 (1998).
[20] J. Hwang, A. M. Clausen, H. Cao, and P. M. Voyles, J. Mat. Res. **24**, 3121 (2009).
[21] R. K. Dash, P. M. Voyles, J. M. Gibson, M. M. J. Treacy, and P. Keblinski, J. Phys: Cond. Mat. **15**, S2425 (2003).
[22] P. Biswas, R. Atta-Fynn, and D. A. Drabold, Phys. Rev. B **69**, 195207 (2004).
[23] T. C. Petersen, I. Yarovsky, I. Snook, D. G. Mcculloch, and G. Opletal, Carbon **41**, 2403-2411.
[24] S. N. Bogle, P. M. Voyles, S. V. Khare, and J. R. Abelson, J. Phys. Cond. Mat. **19**, 455204 (2007).
[25] P. M. Voyles, N. Zotov, S. M. Nakhmanson, D. A. Drabold, J. M. Gibson, M. M. J. Treacy, P. Keblinski, J. Appl. Phys. **90**, 4437 (2001).
[26] F. Yi, P. Tiemeijer, and P. M. Voyles, J. Elec. Mic. **59 (Suppl.)**, S15 (2010).
[27] F. Yi, and P. M. Voyles, Ultramicroscopy **111**, 1375 (2011).
[28] J. Hwang, and P. M. Voyles, Microsc. Microanal. **17**, 67 (2011).
[29] J. M. Gibson, M. M. J. Treacy, and P. M. Voyles, Ultramicroscopy **83**, 169 (2000).
[30] A. Howie, Ultramicroscopy **98**, 73 (2004).
[31] L.A. Freeman *et al.,* The Structure of Non-Crystallized Materials (Taylor and Francis, London, UK, 1976).
[32] R. L. McGreevy, J. Phys.: Condens. Matter **13**, R877 (2001).
[33] V. I. Tkatch, A. I. Limanovskii, S. N. Denisenko, and S. G. Rassolov, Mat. Sci. Eng. A **323**, 91 (2002).

[34] A. Slipenyuk, and J. Eckert, Scripta Materialia **50**, 39 (2004).
[35] W. Dmowski, C. Fan, M. L. Morrison, P. K. Liaw, and T. Egami, Mat. Sci. Eng. A **471**, 125 (2007).
[36] J. Wen, Y. Q. Cheng, J. Q. Wang, and E. Ma, J. Appl. Phys. **105**, 043519 (2009).
[37] S. G. Hao, M. J. Kramer, C. Wang, K. Ho, S. Nandi, A. Kreyssig, A. Goldman, V. Wessels, K. Sahu, K. F. Kelton, R. Hyers, S. Canepari, J. Rogers, Phys. Rev. B **79**, 104206 (2009).
[38] A. S. Clarke, and H. Jónsson, Phys. Rev. E **47**, 3975 (1993).
[39] URLWillBeInsertedByPublisher
[40] Inorganic Crystal Structure Database, http://www.fiz-karlsruhe.de/icsd.html
[41] P. W. Stephens, and A. I. Goldman, Phys. Rev. Lett. **56**, 1168 (1986).
[42] C. Zhang, L. Hu, Y. Yue, and J. C. Mauro, J. Chem. Phys. **133**, 014508 (2010).
[43] U. R. Pedersen, T. B. Schrøder, J. C. Dyre, and P. Harrowell, Phys. Rev. Lett. **104**, 105701 (2010).
[44] H. Tanaka, T. Kawasaki, H. Shintani, and K. Watanabe, Nat. Mat. **9**, 324 (2010).

Figure 1. (a) DSC data for as-quenched and annealed samples.

Figure 2. (a) Experimental $V(k)$ from the as-quenched and annealed samples and simulated $V(k)$ from the models. (b) Total x-ray $S(k)$ from experiment and calculated from the EAM only and HRMC models, offset for clarity.

Figure 3. (a) Histograms of the VP categories for the HRMC and EAM-only models. Gray are Zr-center VPs, orange are Cu-centered, and green are Al-centered. (b) CNA indices for the models. Error bars are the square root of the number of VPs or CNAs counted.

Figure 4. (a) A region including the crystal-like supercluster of the 300 °C, 60 minute annealed model. (b) A region of the EAM-only model the same size. The atoms are colored by the fraction of pentagons in their VPs. (c) CNA indices of the crystal-like supercluster and the remainder of the 300 °C, 60 minute annealed model. (d) A chain icosahedral supercluster from the yellow circled region in (a). VP indices are shown for the central atoms, and atoms are colored by species.

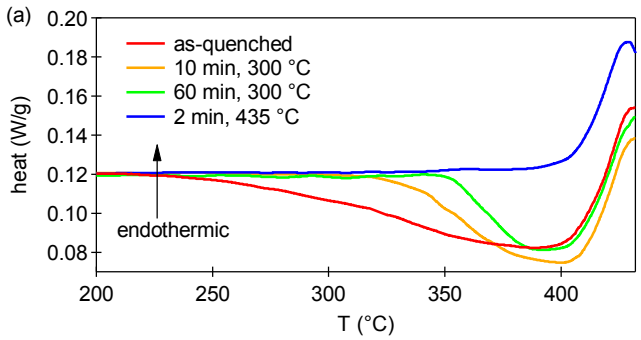

Figure 1

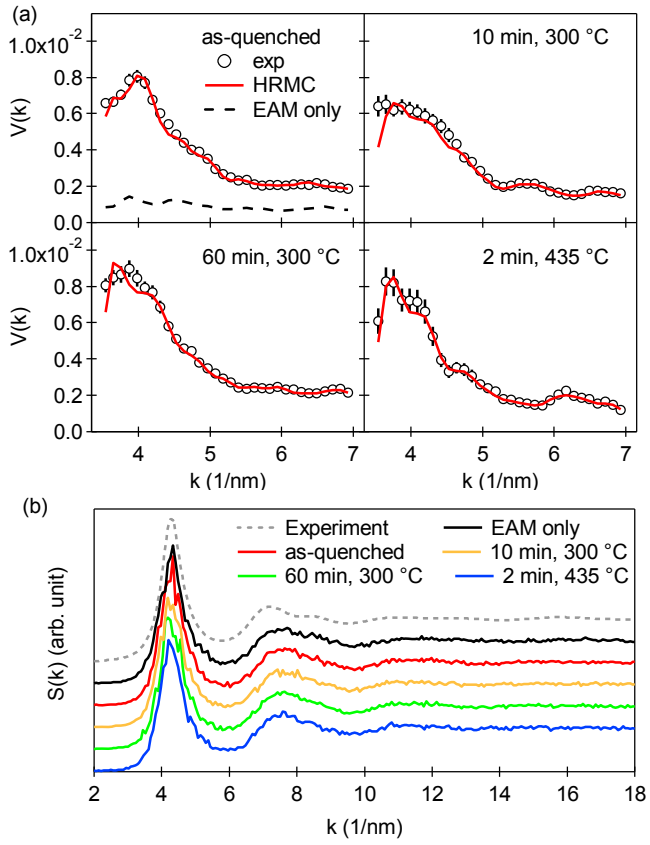

Figure 2

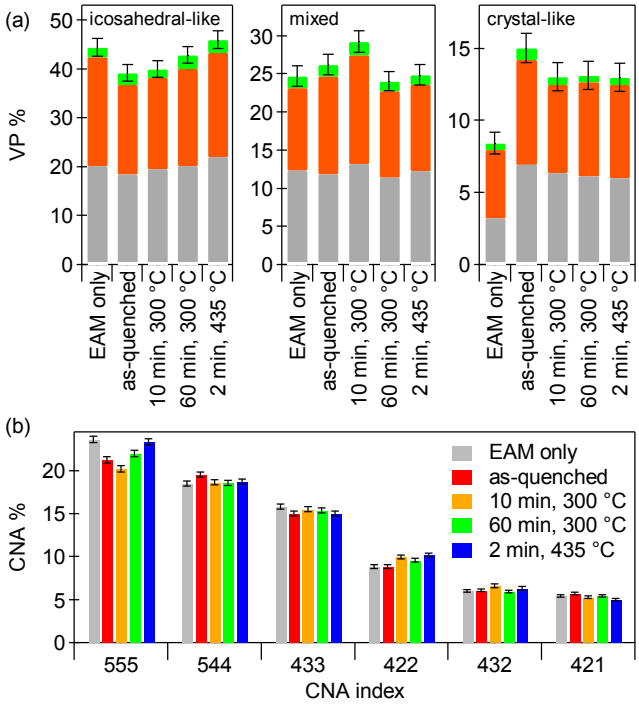

Figure 3

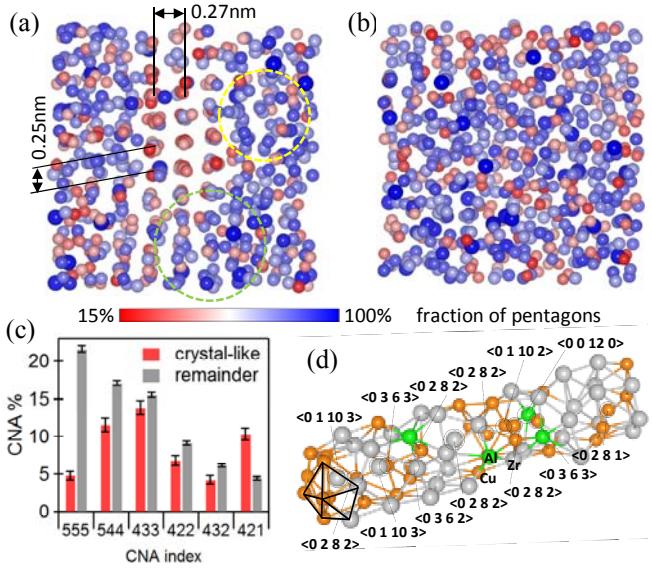

Figure 4